Astron. Astrophys. 341, 882–895 (1999)

ASTRONOMY AND ASTROPHYSICS

Vibrationally excited HC_3N toward hot cores

F. Wyrowski[1,2,⋆], **P. Schilke**[2], **and C.M. Walmsley**[3]

[1] I. Physikalisches Institut der Universität zu Köln, Zülpicherstrasse 77, D-50937 Köln, Germany
[2] Max-Planck-Institut für Radioastronomie, Auf dem Hügel 69, D-53121 Bonn, Germany
[3] Osservatorio Astrofisico di Arcetri, Largo E.Fermi 5, I-50125 Firenze, Italy

Received 15 July 1998 / Accepted 22 October 1998

Abstract. We report IRAM 30-m observations of vibrationally excited rotational transitions of HC_3N toward a sample of six ultra–compact HII regions. In addition, Effelsberg 100-m and Plateau de Bure Interferometer measurements were conducted toward the region G10.47+0.03. We detected the $v_7 = 1$ state of cyanoacetylene toward all six regions and the $v_6 = 1$ line toward five of them. Toward G10.47+0.03, we detected lines from 11 different vibrationally excited states with excitation energies up to 1600 K above ground. Of these, six are first detections. We also have detected several transitions of ^{13}C substituted cyanoacetylene in the $v_6 = 1$, $v_7 = 1$, and $v_7 = 2$ states and provide improved rest frequencies for several of these. The population distribution of the vibrationally excited HC_3N molecules is analyzed and it is concluded that our results are consistent with thermalised level populations at a temperature of 270 K. From the interferometer results we find the source of HC_3N emission to be coincident with NH_3(4,4) and CH_3CN emission within the positional error of $1''$.

In an appendix, we report the first astronomical detection of lines from vibrationally excited HNCO in G10.47+0.03.

Key words: ISM: clouds – ISM: H II regions – ISM: molecules – radio lines: ISM

1. Introduction

Massive O-B stars form in dense condensations within molecular clouds. The high dust extinction ($A_V \sim 1000$) within such condensations obscures their innermost parts in the near and mid-IR making it difficult to study the internal structure in these wavelength regions. Recently it has been recognized that one tracer for O-B stars in the earliest phases of their evolution is the presence of emission from high excitation molecular lines. Such molecular hot cores are usually found in the neighborhood of compact HII regions and have masses in the range 10-3000 $M_\odot$ and temperatures of order 200 K (Churchwell 1991). One of the important characteristics of these objects is their internal radiation field or (equivalently) the distribution of dust temperature. Since the infrared radiation in the interior is not directly observable, due to the extinction mentioned above, one has to resort to indirect methods. One such method is observing rotational transitions at radio wavelengths excited due to radiative pumping by IR dust photons.

Most of the work done so far has been concerned with the "Hot Core" in the Orion KL region and Sgr B2. Churchwell et al. (1986) analyzed HNCO as a probe of FIR radiation. Vibrationally excited HC_3N has been studied by Goldsmith et al. (1982, 1985). A recent interferometer molecular line survey of Orion KL by Blake et al. (1996) with OVRO gives insight into the spatial distribution of HNCO and vibrationally excited HC_3N. Other examples of vibrationally excited molecules studied in star formation regions are HCN (Ziurys & Turner 1986), NH_3 (Mauersberger et al. 1988), CH_3CN (Clark et al. 1976; Olmi et al. 1996a), and maser emission of SiO (Snyder & Buhl 1974).

In the last few years, new hot core sources have joined the classical ones, among them are the particularly interesting young embedded objects associated with the UC HII regions G10.47+0.03 and G31.41+0.31. They have been studied using the VLA in high excitation ammonia lines (Cesaroni et al. 1994, 1998) and with both the 30-m telescope and Plateau de Bure interferometer in methyl cyanide (Olmi et al. 1996a, b). Both sources have also been observed in recent studies of $^{15}NH_3$ (Wyrowski & Walmsley 1996) and of $C^{17}O$ (Hofner et al. in preparation). The sources are associated with hot, high column density molecular gas with characteristics similar to those of the hot core seen toward the Orion KL region but much more massive. From the dust emission the gas masses of the compact cores are found to be of the order of 2000 $M_\odot$ within a region of about 0.05 pc. As contrasting cases, we decided to observe W3(H_2O) (a hot core comparable to Orion-KL) and the cores G10.62–0.38, G29.96–0.02, and G34.26+0.15 (Churchwell et al. 1990).

In this article, we present 30-m telescope measurements of vibrationally excited HC_3N toward this sample of hot cores. Since these single dish results do not provide direct information on the position and size of the source responsible for the vibrationally excited lines, we have supplemented the 30-m data with Plateau de Bure Interferometer observations at 110 GHz

Send offprint requests to: F. Wyrowski, Maryland address
⋆ *Present address:* University of Maryland, Department of Astronomy, College Park, MD 20742, USA
Correspondence to: wyrowski@astro.umd.edu

Table 1. Wavelengths of the IR pump radiation of different vibrational modes of HC_3N, their Einstein coefficients and critical densities.

Transition	$\lambda_{\rm EXC}$ (μm)	A_{ul} (s^{-1})	n_{cr} cm^{-3}	vibration
$v_4 = 1-0$	11	0.003	$2 \cdot 10^{10}$	C-C stretch
$v_5 = 1-0$	15	2.2	$7 \cdot 10^{12}$	HCC bend
$v_6 = 1-0$	20	0.15	$3 \cdot 10^{11}$	CCN bend
$v_7 = 1-0$	45	$6 \cdot 10^{-4}$	$4 \cdot 10^{8}$	CCC bend

of the vibrationally excited HC_3N emission toward the spectacular source G10.47+0.03. It is also of interest to get information on the wavelength dependence of the line intensity and hence we have obtained Effelsberg 100-m observations of the vibrationally excited HC_3N transitions at 36 and 45 GHz for comparison with the higher frequency data.

2. Line frequencies for vibrationally excited HC_3N

The linear pentatomic molecule cyanoacetylene has seven modes of vibration, four stretching modes and three bending modes which are doubly degenerate (Mallinson & Fayt 1976). An overview of the various fundamental vibrations is given in Table 1. The stretching modes ν_1, ν_2, ν_3, which lie more than 3000 K above ground, are omitted. Besides the fundamental modes of vibration also overtones and combinations modes can be observed. A level diagram of all modes lower than 1700 K is shown in Fig. 1. Several of these modes are coupled by anharmonic resonances (Yamada & Creswell 1986). Laboratory studies of the infrared spectrum have been made firstly by Turrel et al. (1957) and more accurately by Mallinson & Fayt (1976) who determined band centers for all seven fundamentals with high precision. The first interstellar detection of vibrationally excited states of this molecule was by Clark et al. (1976) toward the Orion hot core.

Since most of the vibrationally excited rotational lines observed by us are first detections in interstellar space, we would like to discuss briefly how the rest frequencies were obtained with the help of the molecular constants derived from laboratory measurements. These extrapolations were necessary to identify observed lines that lie outside the frequency ranges analyzed in the laboratory, and to predict frequencies in other wavelength ranges for future studies.

For the purpose of determining the frequencies of the transitions observed astronomically, we have used where possible the effective rotational constants $B_{\rm eff}$ and $D_{\rm eff}$, which Yamada & Creswell (1986) used to fit their laboratory measurements with sufficient accuracy for all the different levels shown in Fig. 1. This accounts for l-type doubling and resonance interaction between different vibrational levels. We thus used the equation:

$$\nu = 2B_{\rm eff}(J+1) - 4D_{\rm eff}(J+1)^3 \quad (1)$$

These effective constants were only available for the main isotopomer. We calculated the frequencies of the less abundant isotopomeric species with the help of the parameters B_0, D_0,

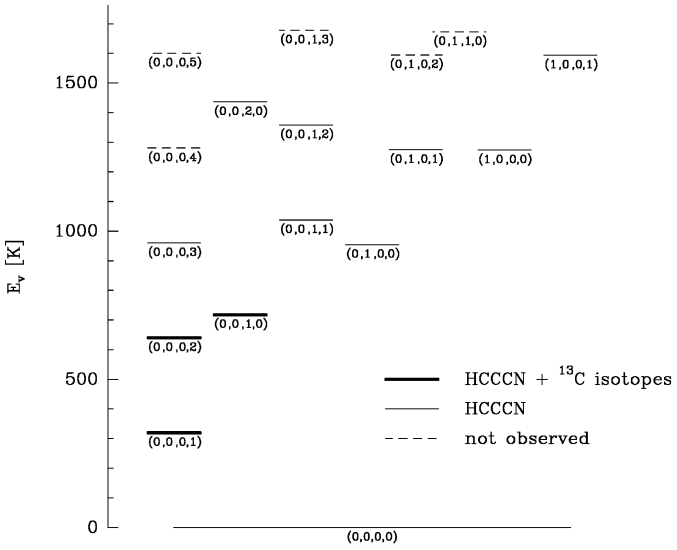

Fig. 1. Vibrational energy levels of HCCCN. v_4 is the quantum number of the lowest stretching vibration, and v_5, v_6, v_7 are bending vibrations. All detected lines are marked and the remaining were not covered by our observing bands.

Table 2. Molecular constants of HC_3N for the observed isotopomer taken from Mallinson & de Zafra (1978).

Constant	HCCCN	$HC^{13}CCN$	$HC^{13}CCN$	$HCC^{13}CN$
B_0/MHz	4549.058	4408.438	4529.755	4530.195
α_5/MHz	−1.813	−1.387	−1.558	−1.552
α_6/MHz	−9.262	−8.960	−9.075	−8.983
α_7/MHz	−14.605	−14.067	−14.020	−14.184
q_5/MHz	2.570	2.428	2.519	2.516
q_6/MHz	3.582	3.367	3.593	3.635
q_7/MHz	6.538	6.175	6.579	6.529
D_0/kHz	0.5444			

α_i, and q_i determined from the analysis of transitions in the 26.5–40.0 GHz region by Mallinson & de Zafra (1978) which are given in Table 2:

$$B_v = B_0 - \alpha_i \quad (2)$$

$$\nu_0 = 2B_v(J+1) - 4D_0(J+1)((J+1)^2 - 1) \quad (3)$$

$$\nu = \nu_0 \pm q_i(J+1) \quad (4)$$

The accuracy of extrapolating this fit of the low frequency transitions to high frequency transitions in the range from 3 to 1.3 mm is a priori unknown, but we will see in Sect. 4 that this procedure works surprisingly well and leads to the identification of ^{13}C substituted HC_3N in vibrationally excited states without ambiguity.

3. Observations

The bulk of our observations were carried out in July 1996 using the IRAM 30-m telescope on Pico Veleta. However, we also carried out supplementary observations of vibrationally excited cyanoacetylene toward G10.47+0.03 using the Effelsberg

100-m telescope operated by the Max-Planck-Institut für Radioastronomie (MPIfR) and the Plateau de Bure interferometer (PdBI) operated by IRAM. In this section, we discuss these in turn.

3.1. 30-m observations

We observed simultaneously at 3, 2, and 1.3 mm with half power beam widths of 22″, 16″, and 12″, respectively. Lists of the observed sources and frequencies are given in Tables 3 and 4. The main targets were the sources G10.47+0.03, G31.41+0.31, and W3(H_2O), but some other sources were observed in a few frequency bands as well. In the following tables, the sources are distinguished by the numbers given in the last column of Table 3.

We used the facility 3 mm, 2 mm, and 1.3 mm (G1 and G2) SIS receivers with system temperatures of 300–450 K, 650–900 K, and 800–3000 K, respectively, depending on weather and elevations. The alignment between the different receivers was checked through continuum cross scans on planets and found to be accurate to within 2″.

Our spectrometers were an autocorrelator with 1633 channels and 0.32 MHz resolution and two filter-banks with 1 MHz resolution and 512 channels. This led to typical velocity resolutions between 1 and 2 $\mathrm{km\,s^{-1}}$. All lines have been observed in the lower sideband with typical sideband rejections of 30, 10, 20 dB at 3, 2, and 1.3 mm, respectively. With the filter banks, we covered 500 MHz centered on the frequencies given in Table 4.

The wobbling secondary mirror was used with a beam throw of 120″ and a frequency of 0.25 Hz resulting in spectra with linear baselines. To obtain main beam brightness temperature as intensity scale, the antenna temperature has been multiplied by the ratio of the forward and the main beam efficiency which were taken from Table A1 of the 30-m manual (Wild 1995).

The focus was checked at the beginning of each night on Jupiter or Saturn. Pointing was checked hourly by cross scans on planets, G10.62–0.38, and W3(OH) and was found to be good within 4″.

3.2. Effelsberg 100-m observations

Using the 100-m telescope, we observed the J=4–3 and J=5–4 transitions of HC_3N at 36 and 45 GHz, respectively. The 36 GHz observations were carried out in two sessions in Jul./Aug. 1997 and the 45 GHz observations in Apr. 1998. The frontends were the facility 1 cm and 7 mm HEMT receivers with receiver temperatures of 120 and 70 K, respectively. Our spectrometer was a 8192 channel autocorrelator which we used with 8 overlapping subunits of 80 MHz bandwidth to cover a total of 490 MHz. The resulting spectral resolution was 0.3 MHz after smoothing the data to increase the signal-to-noise. The beams at the frequencies of the HC_3N lines were 25″ and 20″. Pointing was checked at roughly hourly intervals by means of continuum scans through G10.62–0.38. We found the pointing to be accurate to within 4″. Our calibration was based upon the continuum scans through G10.62–0.38, assuming a flux density of 4.3 Jy at 43 GHz (Wood et al. 1988) corresponding to a main-beam brightness temperature of 6.1 K. The relative calibration between the 36 and 45 GHz data was established with the help of the simultaneously observed H52α and H56α recombination lines assuming their intensities to scale simply inversely with frequency.

Table 3. Observed sources

Source	α_{2000}	δ_{2000}	$v_{\rm LSR}$ ($\mathrm{km\,s^{-1}}$)	
G10.47+0.03	18:08:38.28	−19:51:50.0	+67.0	1
G10.62−0.38	18:10:28.67	−19:55:50.1	+67.0	2
G29.96−0.02	18:46:03.78	−02:39:21.9	+98.7	3
G31.41+0.31	18:47:34.32	−01:12:45.8	+97.0	4
G34.26+0.15	18:53:18.61	+01:14:57.3	+59.1	5
W3(H_2O)	02:27:04.63	+61:52:24.7	−49.0	6

Table 4. Frequency setup

$\nu_{\rm center}$ in GHz	observed sources
109.41	1,4
110.095	1-6
154.23	1,3,4,6
154.85	1-6
218.97	1,4,6
228.1	1,4

3.3. Plateau de Bure observations

We observed the J =12–11 transition of HC_3N in Jul.–Oct. 1997 using the Plateau de Bure Interferometer with 4 antennas in the C2/C1/B1/B2 configurations (a description of the instrument is given by Guilloteau et al. 1992). The primary beam of the antenna at a frequency of 109.25 GHz was 44″ and the synthesized beam was 5.2×1.6″. The correlator was split into 6 units of 80 MHz width and 128 channels to cover the frequency range from 109.0 to 109.5 GHz in the upper sideband and from 106.0 to 106.5 GHz in the lower sideband of the SIS receivers. This correlator setup was slightly changed after observation of the first configuration to cover all HC_3N lines in the frequency range. This lead to a non-uniform UV-coverage across the total frequency range. The resulting spectral resolution was 1.7 $\mathrm{km\,s^{-1}}$. To calibrate the phase, nearby point sources (1730-130, 1908-201) were observed every 5 minutes. The bandpass calibration was carried out using 3C273, 2230+114, and 1730-130.

The absolute flux scale was checked by observations of MWC 349 (assuming a flux of 1.1 Jy at 109.3 GHz) and is found to be correct within 15%. A continuum map was built using "line-free" spectral ranges at 109.05, 109.2, and 109.33 GHz. The total continuum flux found is 0.9 Jy. As another check we determined the flux of the continuum of G10.47+0.03 for each observing day and found a day to day variation of 10%.

Table 5. Observed HC_3N(17–16) intensities. Note that the v_7 and v_6 lines at 155035 MHz are blended and the total intensity is given.

ν (MHz)	Vib. state	Source	$\int T_{\rm MB}\,dv$ (K km s^{-1})
154657.281	(0,0,0,0)	G10.47+0.03	43.0±1.0
		G10.62−0.38	46.0±0.4
		G29.96−0.02	22.6±0.4
		G31.41+0.31	37.5±0.9
		G34.26+0.15	49.6±0.9
		W3(H_2O)	13.1±0.2
154910.969	$(0,0,1,0)^{1-}$	G10.47+0.03	6.6±0.7
		G10.62−0.38	0±0.2
		G29.96−0.02	0.6±0.1
		G31.41+0.31	1.7±0.4
		G34.26+0.15	1.7±0.3
		W3(H_2O)	0.1±0.05
155032.734	$(0,0,1,0)^{1+}$	G10.47+0.03	23.2±0.5
+155037.359	$(0,0,0,1)^{1-}$	G10.62−0.38	0.5±0.2
		G29.96−0.02	6.1±0.3
		G31.41+0.31	11.0±0.3
		G34.26+0.15	5.5±0.7
		W3(H_2O)	2.6±0.1

Due to the low elevation of the source and only modest weather conditions during summer, the phase noise lead to decorrelation on the longer baselines resulting in a "radio seeing" of about 1.″5.

4. Observational results

In this section, we present our observations starting with the 30-m results.

We observed the J=17–16 HC_3N lines near 154 GHz toward all six of the sources in Table 3. Within this sample, the most spectacular case is G10.47+0.03 for which we have also measurements at 3 and 1.3 mm. We summarize these and discuss the line identifications. Then, we present our 100-m measurements of two low J transitions toward G10.47+0.03. Finally we discuss the Plateau de Bure results of the J =12–11 transition of HC_3N.

4.1. The J=17–16 HC_3N observations near 154 GHz

Near 154 GHz, we detected HC_3N(17–16) in its ground and lowest (v_7) vibrationally excited states toward all six sources and the v_6 state in all sources except G10.62–0.38. The observed line parameters are given in Table 5 and the spectra are shown in Fig. 2. To analyze the different excitation conditions in the sources, we plotted the ratios of the integrated line intensities against each other in Fig. 3. For comparison purposes, the well-known hot core sources Orion KL and Sgr B2N were added with their line intensities taken from the literature (Goldsmith et al. 1985 and de Vicente 1994). Since the vibrational ground state line of HC_3N is expected to be dominated by more extended emission, the ratio between the v_7 and the ground state is not a measure of the vibrational temperature but rather a rough measure of the relative amount of molecules in vibrationally excited states in the whole region, whereas the ratio of the intensities I_{v_6}/I_{v_7} in the excited states v_6 and v_7 can be converted to a vibrational temperature $T_{\rm vib}$ of the hot core assuming optically thin conditions:

$$\frac{I_6}{I_7} = \exp\left(-\frac{\Delta E_{67}}{kT_{\rm vib}}\right) \quad (5)$$

where ΔE_{67} denotes the energy difference between the v_6 and v_7 states. Ratios of 0.1, 0.2, and 0.4 then correspond to $T_{\rm vib}$ =170, 250, and 430 K, respectively. This assumes optically thin emission which is, as discussed below, not valid in

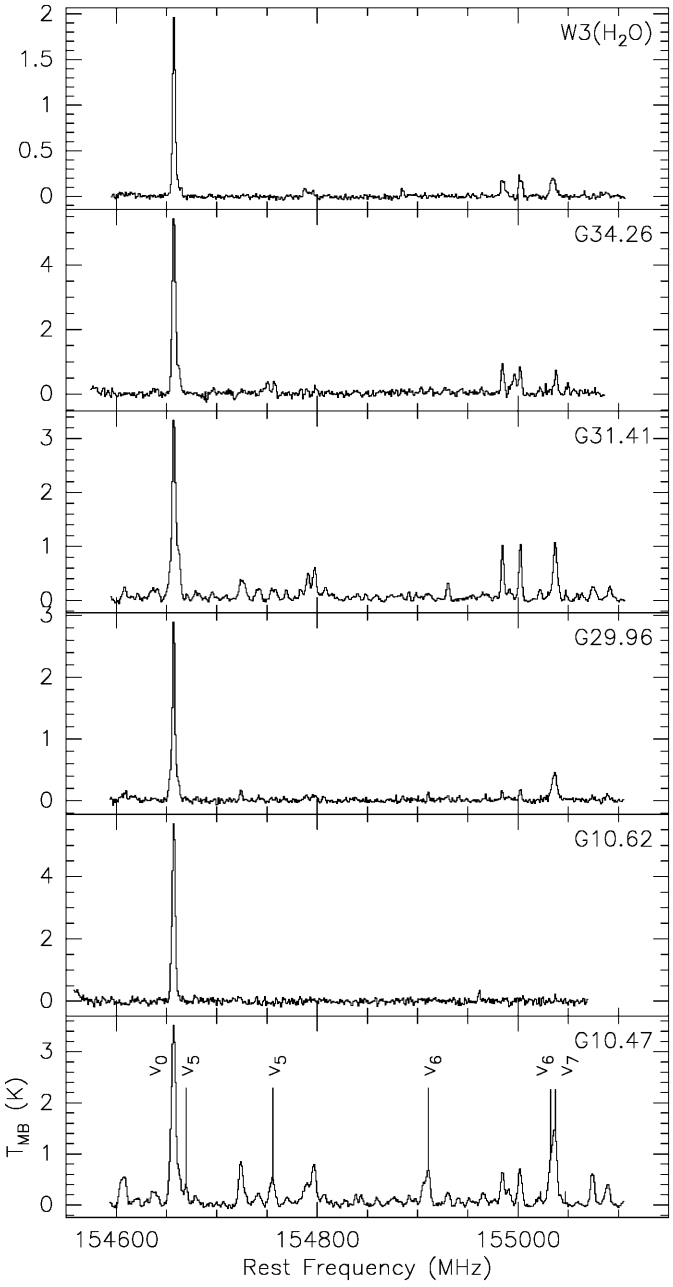

Fig. 2. HC_3N (17–16) spectra at 155 GHz toward all observed sources.

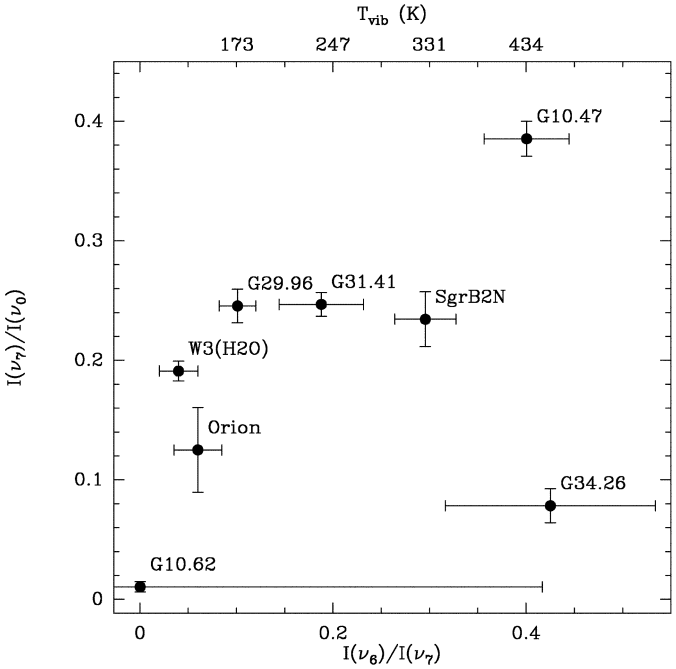

Fig. 3. Ratios of line intensities in the vibrational states v_0, v_7 and v_6 toward the observed hot cores and, additionally, for the hot cores Orion KL and Sgr B2N where the values of the (12–11) intensities are taken from Goldsmith et al. (1985) and de Vicente (1994).

G10.47+0.03 in which even ^{13}C isotopomer lines of HC_3N were observed, but a good approximation for the other sources, in which we don't find any ^{13}C isotopomer lines. There is a trend for higher vibrational temperatures with a larger amount of vibration relative to the extended ground state emission. The only exception is G34.26+0.15. In this complex, UC HII regions of different morphologies are found (e.g. Gaume et al. 1994). Hence, star formation in different evolutionary states is present within our 30-m beam. The high vibrational temperature could belong to the dense cores associated with the water masers and the high ground state emission to the bulk of a halo forming surrounding gas (see the discussion of Garay & Rodriguez 1990 on different ammonia structures in this source). In G10.62–0.38, the vibrationally excited emission is very weak. There is a trend for higher excitation to be found in higher mass sources with the moderately massive cores W3(H_2O) and Orion KL at the lower end, and the very massive cores Sgr B2N and G10.47+0.03 at the higher end. The position of G10.47+0.03 is exceptional in comparison to the other sources. In this source, many other vibrationally excited states were detected as discussed in detail in the next section.

4.2. Vibrationally excited HC_3N in G10.47+0.03

We detected rotational transitions in eleven vibrationally excited states of HC_3N (six of these are detected for the first time in interstellar space) toward the hot core associated with the UC HII region G10.47+0.03. This allows the most detailed study of vibrational (as opposed to rotational) excitation in a molecular cloud so far. Since the line blending problem becomes severe at 1.3 mm, the HC_3N lines are most easily identified at 3 and 2 mm. We show the spectra obtained at these wavelengths together with identifications and a formal fit with T=500 K in Figs. 4 and 5 (details about the fit procedure are given by Schilke & Phillips 1998, in preparation). Lines from vibrationally excited HNCO are detected as well and will be discussed in Appendix A.

We have detected transitions in the (v_4, v_5, v_6, v_7) = (0,0,0,1), (0,0,0,2), (0,0,0,3), (0,0,1,0), (0,0,2,0), (0,0,1,1), (0,0,1,2), (0,1,0,0), (0,1,0,1) bending vibrational states and also the (1,0,0,1) and (1,0,0,0) stretching vibrational levels. One may compare with Orion, where, despite deep searches, only the (0,0,0,1), (0,0,0,2) and (0,0,1,0) states have been found (Clark et al. 1976; Goldsmith et al. 1982, 1985; Blake et al. 1987). An overview of the detected states is shown in Fig. 1 where one sees they range up to more than 1500 K above ground. Lines from levels marked as "not observed" lay outside our observing bands. The observed intensities of the lines are given in Table 6.

An example of modes with two quanta of vibration excited is shown in the upper panel of Fig. 6. The combination mode (0,1,0,1), which lies about 1300 K above ground, is split into four components with $|l|$=0, 2. This splitting is due to l-type doubling and, additionally, due to anharmonic resonances in the (1,0,0,0)-(0,1,0,1)-(0,0,2,0)-(0,0,0,4) system (Yamada & Creswell 1986). From this four state resonance, we also see two $v_6 = 2$ lines about 1450 K above ground. Here, the splitting of the $|l|$=2 lines is too small to be observed and both lines overlap resulting in a relatively high intensity. One should note the excellent coincidence of line frequencies measured in the laboratory and astronomically which gives strong confidence in the identification of these lines. Evidence for (0,0,1,1) lines is found in a 1.3 mm spectrum near the $C^{18}O$(2–1) line (Hofner et al. in prep.). Fig. 7 shows three spectral features close to the predicted frequencies. Small errors in the prediction are possible because of large perturbation terms in the Hamiltonian (Yamada & Creswell 1986). But the detection is further confirmed by more lines from that mode observed with the 100-m telescope (Fig. 8). Also all lines in our observed bands with three quanta of vibration excited are clearly identified ((0,0,1,2) and (0,0,0,3)) in the lower panel of Fig. 4. The highest lying detected lines are three lines in the (1,0,0,1) mode 1600 K above ground. Although the signal-to-noise of these detections is rather low (3–5 σ), all three lines are very well reproduced by our LTE fit (Figs. 4 and 5, 109306.7, 109469.4, 154844.8 MHz) with T=500 K. The line at 155074.9 GHz seems to be blended with an U-line. A line in the pure stretching mode v_4 is detected at 154443.8 MHz. A possible blend with the ethanol $7_{16} - 6_{24}$ line at 154442.7 MHz is believed to be weak (considering the results of Wyrowski 1997, Chapter 5), but there is still an contribution from an unknown, extended spectral feature in the range from 154434 to 154460 MHz. Another detection of a line of the v_4 mode is reported in Sect. 4.4 with the Plateau de Bure interferometer.

Moreover, we have also detected for the first time the v_7 =1,2 and the $v_6 = 1$ states of ^{13}C substituted HC_3N. No DCCCN was found at the position of a (12–11) v_7 line at 110015.4

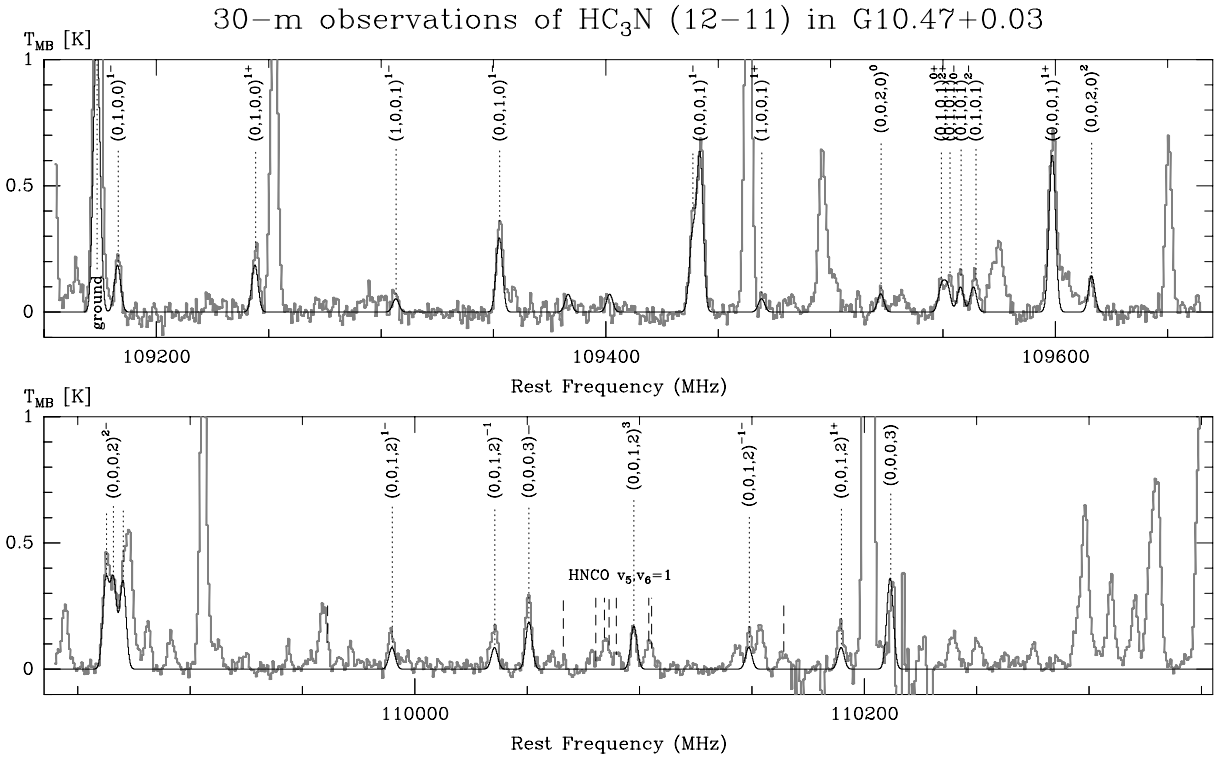

Fig. 4. 30-m spectra of HC_3N(12–11) toward G10.47+0.03. The identified vibrational excited states are marked with dots and their vibrational quantum numbers (v_4, v_5, v_6, v_7). The applied fit to HC_3N assumes one single temperature for all lines of 500 K. Vibrationally excited HNCO is marked with dashes. The strong line at 110.2 GHz is the ^{13}CO line which shows several absorption features caused by the small wobbler throw of 2′.

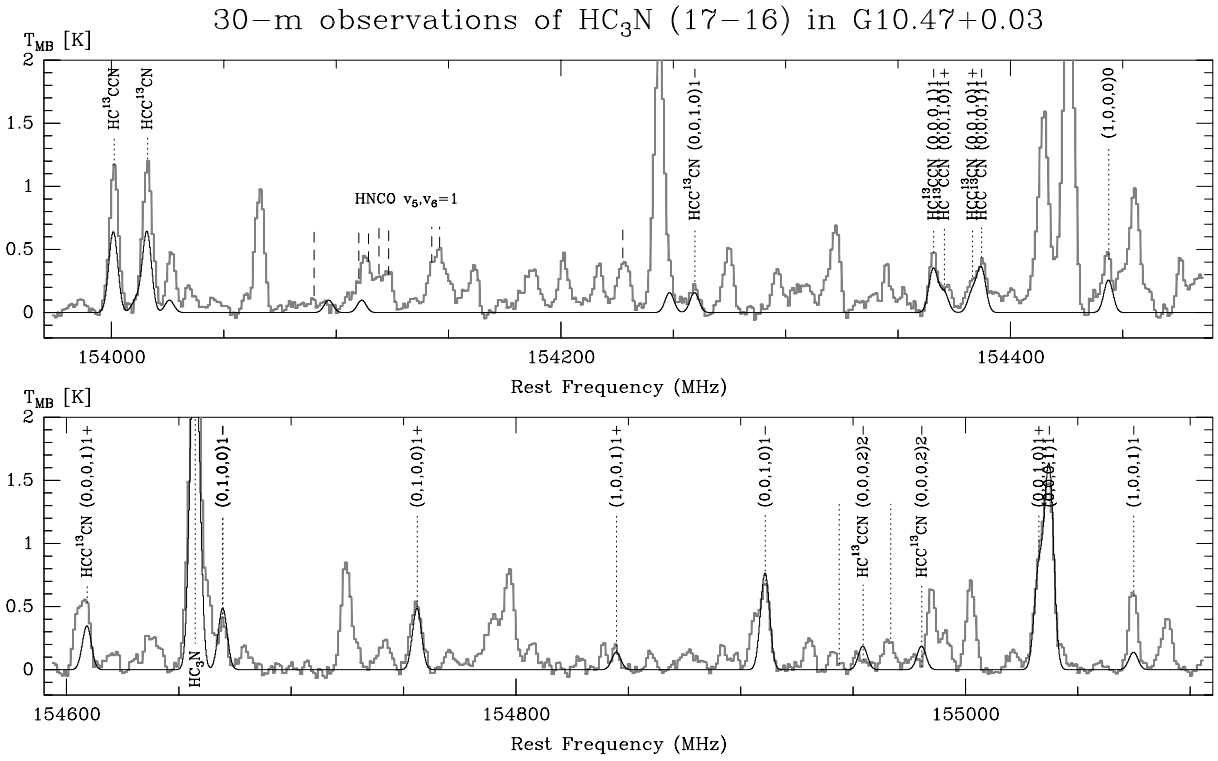

Fig. 5. Same as Fig. 4 but HC_3N(17–16)

Table 6. HC_3N intensities in G10.47+0.03 observed with the 30-m telescope

ν (MHz)	Trans.	Vib. state	$E_{\rm up}$ (K)	$\int T_{\rm MB}\,dv$ (K km s^{-1})
HC_3N				
109182.9	12–11	$(0, 1, 0, 0)^{1-}$	988	2.0
109244.0	12–11	$(0, 1, 0, 0)^{1+}$	988	2.4
109306.7	12–11	$(1, 0, 0, 1)^{1-}$	1627	0.6
109352.8	12–11	$(0, 0, 1, 0)^{1-}$	751	3.7
109438.7	12–11	$(0, 0, 1, 0)^{1+}$	751	3.2
109442.0	12–11	$(0, 0, 0, 1)^{1-}$	354	7.1
109469.4	12–11	$(1, 0, 0, 1)^{1+}$	1627	0.6
109522.5	12–11	$(0, 0, 2, 0)^{0}$	1469	0.7
109549.5	12–11	$(0, 1, 0, 1)^{0+}$	1308	1.1
109552.1	12–11	$(0, 1, 0, 1)^{2+}$	1308	1.3
109558.0	12–11	$(0, 1, 0, 1)^{0-}$	1308	1.3
109563.7	12–11	$(0, 1, 0, 1)^{2-}$	1308	1.4
109598.8	12–11	$(0, 0, 0, 1)^{1+}$	354	7.9
109616.3	12–11	$(0, 0, 2, 0)^{2}$	1469	1.1
109862.8	12–11	$(0, 0, 0, 2)^{0}$	674	4.5
109866.1	12–11	$(0, 0, 0, 2)^{2-}$	674	2.4
109870.3	12–11	$(0, 0, 0, 2)^{2+}$	674	4.7
109990.0	12–11	$(0, 0, 1, 2)^{1-}$	1391	1.4
110035.6	12–11	$(0, 0, 1, 2)^{-1}$	1391	1.8
110051.0	12–11	$(0, 0, 0, 3)^{-}$	994	2.7
110097.6	12–11	$(0, 0, 1, 2)^{3}$	1391	1.3
110148.8	12–11	$(0, 0, 1, 2)^{-1-}$	1391	1.2
110189.8	12–11	$(0, 0, 1, 2)^{1+}$	1392	1.8
110211.4	12–11	$(0, 0, 0, 3)^{3}$	994	2.2
155037.4	17–16	$(0, 0, 0, 1)^{1-}$	387	15.4
219173.8	24–23	$(0, 0, 0, 1)^{1+}$	451	17.3
228303.2	25–24	$(0, 0, 0, 1)^{1-}$	462	18.8
$HCC^{13}CN$				
154259.6	17–16	$(0, 0, 1, 0)^{1-}$	784	1.9
154365.8	17–16	$(0, 0, 0, 1)^{1-}$	386	3.8
154370.6	17–16	$(0, 0, 1, 0)^{1+}$	784	2.4
154969.9	17–16	$(0, 0, 0, 2)^{0}$	706	1.2
$HC^{13}CCN$				
154383.2	17–16	$(0, 0, 1, 0)^{1+}$	784	2.0
154387.2	17–16	$(0, 0, 0, 1)^{1-}$	386	4.1
154943.8	17–16	$(0, 0, 0, 2)^{0}$	706	1.3
154954.5	17–16	$(0, 0, 0, 2)^{2-}$	706	1.2
154966.8	17–16	$(0, 0, 0, 2)^{2+}$	706	1.6

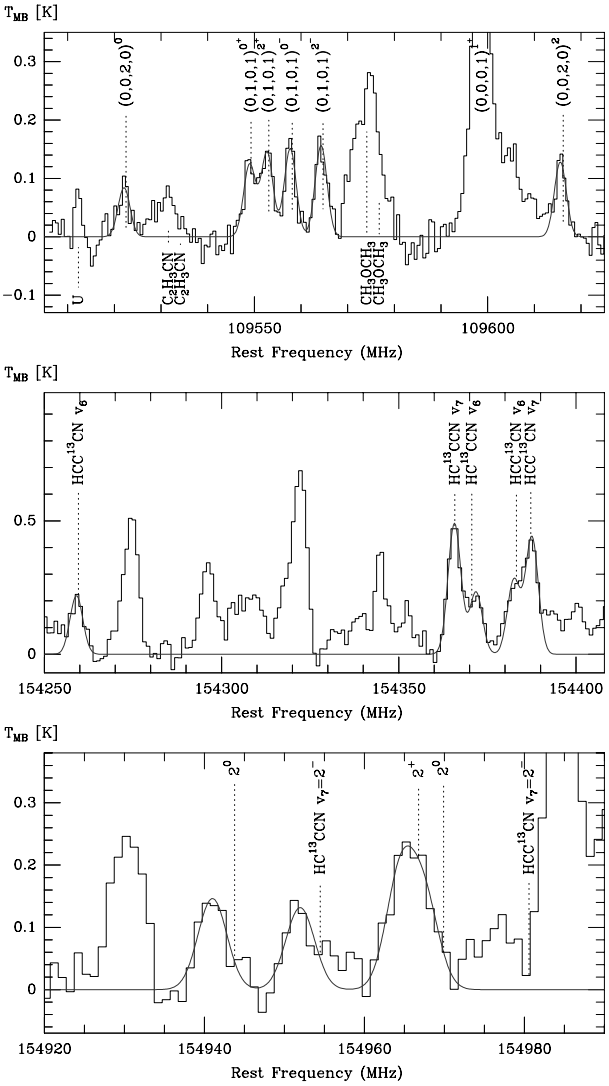

Fig. 6. HC_3N spectra toward G10.47+0.03 showing in the upper panel the combination mode v_5v_7 and the overtone $2v_6$, in the center panel the fundamental modes v_7 and v_6 of two ^{13}C substituted HC_3N species, and in the lower panel their $2v_7$ overtones. The fitted line is a Gaussian fit with the line widths fixed to 8.25 km s^{-1} (the width measured for the v_5 lines) and the frequency and intensity as free parameters.

MHz (rms=20 mK), and only the $HCCC^{15}N$ (12–11) vibrationally ground state line has been observed with the PdBI (see Sect. 4.4). The identifications of these lines is shown in more detail in the middle and lower panels of Fig. 6. The assignments were done according to the frequencies discussed in the last section. The l-type doubling of the $|l|$=2 state was unknown and estimated to be equal to the splitting of the main isotopomer. Predicted and measured frequencies, given in Table 7, agree within a few MHz, which is remarkable since the frequencies are extrapolated from centimeter laboratory measurements. The relatively strong line at 154965 MHz in the lower panel of the figure is presumably due to the blending of two lines of different isotopomers ($HC^{13}CCN$ $v_7 = 2^+$ and $HCC^{13}CN$ $v_7 = 2^0$) and was fitted with two Gaussian lines. In contrast to the lines with only one quantum of vibration excited, the $v_7 = 2$ lines observed show a systematic offset from the predictions. The l-type doubling prediction itself is better than 0.5 MHz.

4.3. The Effelsberg 100-m measurements of HC_3N

Four different vibrationally excited states of HC_3N in the J=4–3 and J=5–4 transitions were detected with the Effelsberg 100-m telescope. The spectra are shown in Fig. 8 and the line intensities are given in Table 8. The lines from states with more than one quantum of vibration are blends of several components and in the table only the total intensity of all components is given.

Table 7. Observed frequencies of vibrationally excited HC_3N isotopomers at 110 GHz with the PdBI and at 154 GHz with the 30-m telescope.

Transition	ν_{obs} (MHz)	$\Delta\nu_{obs}$ (MHz)	O–C (MHz)
$H^{13}CCCN\ v_7 = 1^-$	106063.0	0.6	0.7
$H^{13}CCCN\ v_7 = 1^+$	106211.0	0.5	0.5
$H^{13}CCCN\ v_7 = 2^0$	106473.1	0.4	–1.0
$H^{13}CCCN\ v_7 = 2^{2-}$	106470.2	0.2	–0.5
$H^{13}CCCN\ v_7 = 2^{2+}$	106476.8	0.3	–1.5
$HC^{13}CCN\ v_7 = 1^-$	109125.7	0.1	–0.1
$HC^{13}CCN\ v_7 = 2^0$	109382.1	0.3	–1.3
$HC^{13}CCN\ v_7 = 2^{2-}$	109378.4	0.4	–1.7
$HC^{13}CCN\ v_7 = 2^{2+}$	109386.3	0.3	–1.4
$HCC^{13}CN\ v_7 = 2^0$	109399.7	0.4	–2.1
$HCC^{13}CN\ v_7 = 2^{2-}$	109396.5	0.4	–2.1
$HCC^{13}CN\ v_7 = 2^{2+}$	109404.8	0.3	–1.3
$HCC^{13}CN\ v_6 = 1^-$	154259.1	1.6	–0.5
$HC^{13}CCN\ v_7 = 1^-$	154365.7	0.6	–0.1
$HC^{13}CCN\ v_6 = 1^+$	154371.8	1.5	1.2
$HCC^{13}CN\ v_6 = 1^+$	154382.5	1.6	–0.7
$HCC^{13}CN\ v_7 = 1^-$	154387.6	1.0	0.4
$HC^{13}CCN\ v_7 = 2^0$	154941.0	0.4	–2.8
$HC^{13}CCN\ v_7 = 2^{2-}$	154952.0	0.5	–2.5
$HC^{13}CCN\ v_7 = 2^{2+}$	154964.5	0.9	–2.3
$HCC^{13}CN\ v_7 = 2^0$	154967.5	1.3	–2.4

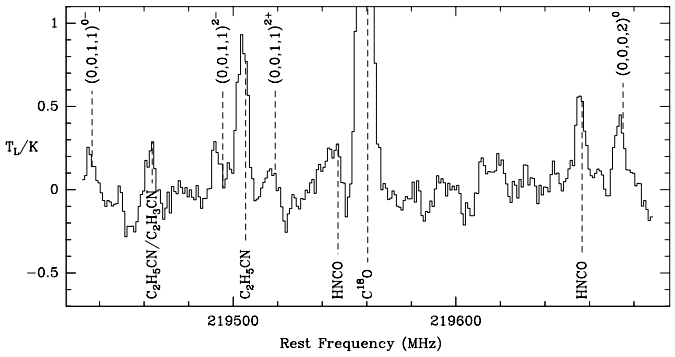

Fig. 7. HC_3N (0,0,1,1) lines detected close to $C^{18}O$(2–1) in G10.47+0.03.

4.4. Plateau de Bure HC_3N J=12–11 results

With the Plateau de Bure Interferometer, we detect a large variety of vibrationally excited states in our J=12–11 observations toward G10.47+0.03. To produce spectra over the whole observed spectral range, we fit a point source model directly to the uv-data. The results are shown in Fig. 9 and a summary of the detected lines is presented in Table 9 which gives the total observed flux density estimated from fitting elliptical Gaussian to the uv-data of the lines to avoid any artifacts introduced during the image processing. Since large phase noise on the longer baselines led to smearing of the emission between 1 and 2 arcsec ("radio seeing"), the total fluxes are more reliable than the peak values. Of particular interest in Fig. 9 is the confirmation of the

Table 8. HC_3N (4–3) and (5–4) intensities in G10.47+0.03 observed with the 100-m

ν (MHz)	Trans.	Vib. state	E_{up} (K)	$\int T_{MB}\,dv$ (K km s^{-1})
36392.33	(4–3)	(0, 0, 0, 0)	4	14.7
36452.06	(4–3)	$(0, 0, 1, 0)^{1-}$	722	.8
36480.72	(4–3)	$(0, 0, 1, 0)^{1+}$	722	
+36481.82	(4–3)	$(0, 0, 0, 1)^{1-}$	324	3.2
36534.13	(4–3)	$(0, 0, 0, 1)^{1+}$	324	2.4
36581.92	(4–3)	$(0, 0, 1, 1)^0$	1042	
+36582.15	(4–3)	$(0, 0, 1, 1)^0$	1042	
+36583.53	(4–3)	$(0, 0, 1, 1)^2$	1042	
+36583.54	(4–3)	$(0, 0, 1, 1)^2$	1042	0.6
36623.24	(4–3)	$(0, 0, 0, 2)^2$	644	
+36623.38	(4–3)	$(0, 0, 0, 2)^2$	644	
+36623.41	(4–3)	$(0, 0, 0, 2)^0$	644	1.6
45490.31	(5–4)	(0, 0, 0, 0)	7	30.9
45564.98	(5–4)	$(0, 0, 1, 0)^{1-}$	724	1.1
45600.80	(5–4)	$(0, 0, 1, 0)^{1+}$	724	
+45602.18	(5–4)	$(0, 0, 0, 1)^{1-}$	327	7.1
45667.56	(5–4)	$(0, 0, 0, 1)^{1+}$	327	5.7
45727.13	(5–4)	$(0, 0, 1, 1)^0$	1044	
+45727.49	(5–4)	$(0, 0, 1, 1)^0$	1044	
+45729.40	(5–4)	$(0, 0, 1, 1)^{2-}$	1044	
+45729.48	(5–4)	$(0, 0, 1, 1)^{2+}$	1044	4.7
45778.95	(5–4)	$(0, 0, 0, 2)^{2-}$	647	
+45779.04	(5–4)	$(0, 0, 0, 2)^{2+}$	647	
+45779.23	(5–4)	$(0, 0, 0, 2)^0$	647	4.5

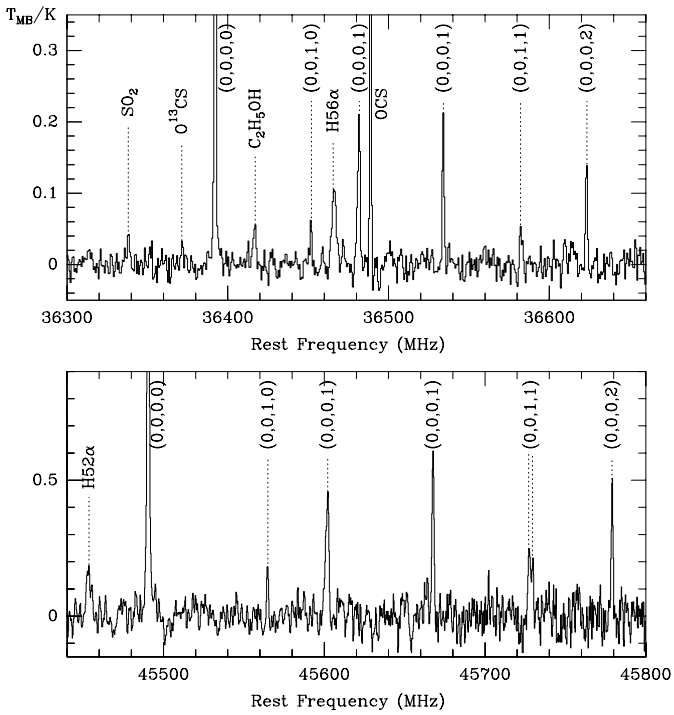

Fig. 8. HC_3N (4–3) and (5–4) lines detected with the Effelsberg 100-m telescope in G10.47+0.03.

detection of the v_4=1 stretching level at 1306 K above ground as well as the detection of the (1,0,0,1) transitions at 1621 K. Another significant result is the detection of several lines of the $v_7 = 1, 2$ levels of ^{13}C isotopomers of HC_3N and the detection of the HCCC^{15}N vibrational ground state.

Predicted and measured frequencies of ^{13}C isotopomers are given in Table 7, and agree, as already the case for the 30-m observations of J =17–16, within a few MHz. Again the $v_7 = 2$ lines observed show a systematic offset from the predictions to lower frequencies.

Our interferometer measurements allow us to determine the position of the source of vibrationally excited HC_3N emission. The position measured by us in the (1,0,0,0) transition at 109023.3 Ghz is $\alpha(2000)$=18:08:38.25, $\delta(2000)$=–19:51:50.5, which is in agreement with the methyl cyanide position (Olmi et al. 1996b), taking the seeing effects of more than 1 arcsec into account. Fig. 10 shows our observation superimposed on the NH_3(4,4) map of Cesaroni et al. (1998). Within our accuracy of our 1″, HC_3N and NH_3 have the same positional origin. To decide, whether the vibrational emission originates from an interface region between hot core and UC HII or is due to a separate, embedded exciting star in the hot core, higher angular resolution observations are needed.

5. Cyanoacetylene level population distribution toward G10.47+0.03

5.1. Optical depths in the vibrationally excited transitions

A first estimate of the vibrational temperature in G10.47+0.03 can be obtained by assuming optically thin conditions and plotting the observed intensities in a Boltzmann plot against excitation for all detected lines in the observed 109 GHz band with the 30-m. Since the lines are observed simultaneously with the same front- and backends, the relative calibration is excellent. The resulting plot is shown in Fig. 11 where one sees that one obtains a reasonable fit with a formal excitation temperature of 485 K (as compared to only 150 K in Orion). We omitted the ground state which forms in a more extended cooler region (see Sect. 4.4) and is deviant by a factor 4. The analysis of the ^{13}C substituted HC_3N, detected at 155 GHz, leads to a similar temperature estimate, but the accuracy of the Boltzmann fit is considerably lower due to the lower signal-to-noise ratio of the detections and due to possible contamination with U-lines (see again Fig. 11).

The ratios of intensities of the main isotopomer and of ^{13}C substitutes can be used to estimate the optical depths of the corresponding transitions. This is done, assuming an ^{12}C/^{13}C abundance ratio X and equal excitation and filling factors for the lines, with the following formula:

$$\frac{I_{12}}{I_{13}} = \frac{1-\exp(-\tau)}{1-\exp(-\tau/X)} \tag{6}$$

The ratio X is a function of galactocentric distance (Dahmen et al. 1995) and is, for a galactocentric distance of 3.0 kpc, 40±15. The resulting optical depths for the v_7 lines of HC_3N(17–16) is then 19±5 and for the v_6 lines 20±10. Since the optical depth is estimated for the 155 GHz range (or J=17) and the vibrational temperature is determined at 110 GHz (or J=12), we have to calculate the expected optical depth at the latter frequency. One can show that for a linear molecule with $T_{\rm ex} \gg h\nu/k$ the ratio of τ at different $J_k(k = i, j)$ is about J_i^2/J_j^2 (see for example Genzel 1992) in LTE and therefore, the optical depth at 110 GHz is approximately 10, consistent with the PdBI results. Hence, the assumption of optically thin lines, which we made to derive a vibrational temperature at 110 GHz, is clearly violated. A better guess can be obtained by considering our results of the (4–3) transition at 36 GHz; here the optical depths in the v_7 line is expected to be of order unity. A Boltzmann fit of the 36 GHz results alone leads to an excitation temperature of 270 ± 35 K.

Besides the population of levels of different vibrational excitation but constant J, we can also study the level population for a constant state of vibration. We detected the v_7 vibrational state at 8, 3, 2, and 1.3 mm and can therefore cover a wide range of rotational excitation within this vibrational mode. The resulting rotational Boltzmann plot for all observed v_7 lines is shown in Fig. 11. In contrast to the very high temperature found for the different vibrationally excited states, the temperature which fits the rotational population of the v_7 mode is only 45 K. This is again misleading since, as discussed above, the optical depth of the lines is considerable and, due to the dependence of optical depth on J, high J lines are depressed and a small rotational temperature is simulated.

Thus we have to interpret the observed intensities taking account of these high optical depths which can be done by including the optical depth into a LTE analysis of the intensities (e.g. Olmi et al. 1996a):

$$\int T\,dv = \frac{8\pi^3\nu\mu^2 S}{3k}\,\frac{N_{\rm tot}}{ZX}\,\exp\left(-\frac{E}{kT}\right)\,G(\tau)\,R(\nu)\,\eta \tag{7}$$

Every transition is characterized by its frequency ν, line strength S and μ, the relevant component of the dipole moment of the molecule. The population of the upper level with energy E of the transition is described by the total column density $N_{\rm tot}$ of the molecule, its partition function as the product of rotational and vibrational part $Z = Z_v Z_r$, the isotopomeric ratio X, and the temperature T. The function $G(\tau)$ corrects for the optical depth of the line (Stutzki et al. 1989):

$$G(\tau) = \int \frac{1-\exp(-\tau g(v))}{\tau\Delta v}\,dv \tag{8}$$

$$\approx \frac{1-\exp(-\tau\prime)}{\tau\prime}, \qquad \tau\prime = 0.679\,\tau^{0.911} \tag{9}$$

The approximation of the integral with this expression is valid for a Gaussian line profile and leads to errors of 15% (4%) for τ in the range of 0.01 to 100 (0.01 to 10). In contrast to the simpler formula using just the line center optical depth (given by setting $\tau\prime = \tau$) suggested by e.g. Turner (1991) and Olmi et al. (1996a), the correction also accounts for the line broadening as function of optical depth. However, this one component approach would produce rectangular line shapes for lines of high optical depth, which are not observed. Indeed, even the high optical depth lines are Gaussian suggesting a more complicated

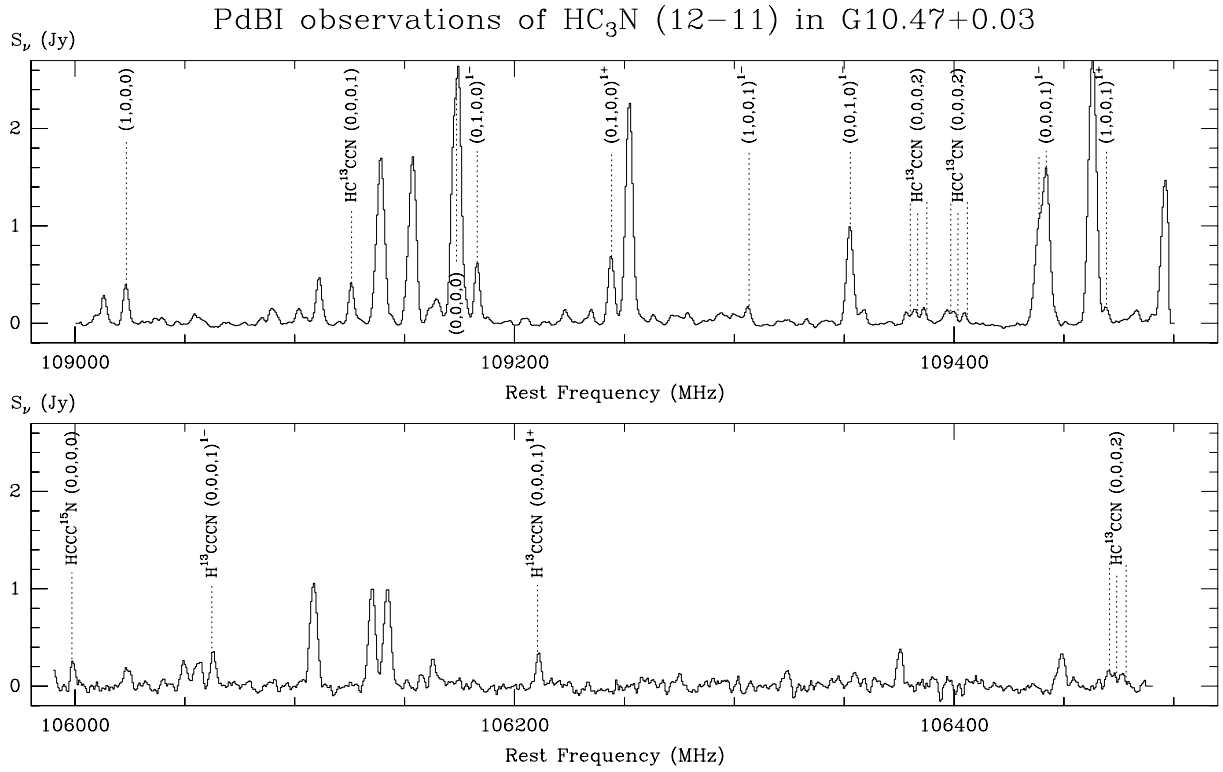

Fig. 9. HC_3N (12–11) lines observed with the PdBI in G10.47+0.03.

line forming process at work, e.g. macroturbulence or large velocity gradients. Having optically thin and thick lines available, the filling factor η can be estimated as well. The optical depth itself, which enters into $G(\tau)$, is given by

$$\tau = \frac{8\pi^3 \nu \mu^2 S}{3k} \frac{N_{\rm tot}}{ZX} \exp\left(-\frac{E}{kT}\right) \frac{1}{T\Delta v} \tag{10}$$

The function $R(\nu)$ in Eq. 7 corrects for the weakening of the spectral line emission by dust absorption due to the very high total column densities of about 10^{25} cm^{-2} involved. We take:

$$R(\nu) = \exp\left[-\tau_{1.3}\left(\frac{\nu}{\nu_{1.3}}\right)^{\alpha}\right] \tag{11}$$

Here the dust absorption optical depth at 1.3 mm is $\tau_{1.3}$ and the frequency dependence of the dust opacity is assumed to be $\alpha = 2$ in the millimeter wavelength range (see Wyrowski et al. 1997 for an observational estimate of the dust opacity index). We include this effect here, since it could also cause the low rotational temperature between v_7 lines with different J and hence frequency (Fig. 11).

Using these formulae, one can search for the minimum of the corresponding reduced least square sum χ^2 of this LTE fit to the n_d observed intensities $I^{obs} = \int T\, dv$:

$$\chi^2 = \frac{1}{n_d - n_p - 1} \sum_{i=1}^{n_d} \left(\frac{I_i^{obs} - I^{mod}}{\Delta I_i}\right)^2 \tag{12}$$

The n_p free parameters of the model are T, $N_{\rm tot}$, θ_S, $\tau_{1.3}$, dv, and (because of the relatively large errors in the assumed isotopomeric ratio) X. The sum is normalized with the number of degrees of freedom $n_d - n_p - 1$. The best fit values of several parameter combinations are given in Table 10. The optical depth of the dust at 1.3 mm $\tau_{1.3}$ is only important for low values of X.

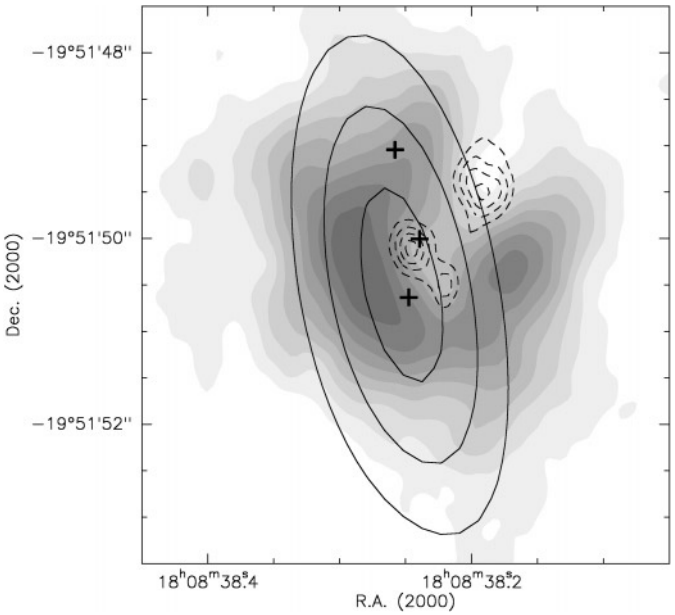

Fig. 10. Overlay of the integrated emission of the HC_3N v_4 line (thin contours: 50, 70, 90% of peak) with the VLA results of Cesaroni et al. (1998) showing the 1.3 cm continuum of the UC HII regions as dashed contours and the main line ammonia (4,4) emission as greyscale. Water masers observed by Hofner & Churchwell (1996) are shown as crosses.

Table 9. HC_3N (12–11) intensities in G10.47+0.03 observed with the PdBI. The given flux is estimated from Gaussian fits to the uv data.

ν (MHz)	Vib. state	$E_{\rm up}$ (K)	$\int S_\nu\, dv$ (Jy km s^{-1})
HC_3N			
109023.3	(1, 0, 0, 0)	1306	5.0
109173.6	(0, 0, 0, 0)	34	102.0
109182.9	(0, 1, 0, 0)$^{1-}$	988	9.3
109244.0	(0, 1, 0, 0)$^{1+}$	988	11.1
109306.7	(1, 0, 0, 1)$^{1-}$	1627	1.9
109352.8	(0, 0, 1, 0)$^{1-}$	751	17.5
109438.7	(0, 0, 1, 0)$^{1+}$	751	
+109442.0	(0, 0, 0, 1)$^{1-}$	354	49.2
109469.4	(1, 0, 0, 1)$^{1+}$	1627	3.0
HCC^{13}CN			
109401.9	(0, 0, 0, 2)	674	6.3
HC^{13}CCN			
109125.8	(0, 0, 0, 1)$^{1+}$	354	6.3
109383.4	(0, 0, 0, 2)	674	5.7
H^{13}CCCN			
106062.3	(0, 0, 0, 1)$^{1-}$	353	5.3
106210.5	(0, 0, 0, 1)$^{1+}$	353	3.8
106474.1	(0, 0, 0, 2)	673	9.5
HCCC^{15}N			
105998.3	(0, 0, 0, 0)	33	2.8

Table 10. Results of LTE model fits including optical depth to the HC_3N data. The $\tau_{\rm cor}$? flag indicates, whether we used Eq. 8 or the simpler expression with $\tau\prime = \tau$ (indicated by no).

$\tau_{\rm cor}$?	X	Δv (km s^{-1})	$\chi^2_{\rm min}$	T (K)	θ_S (arcsec)
no	20	8	1.9	325	1.1
	30		2.3	295	1.0
	40		2.9	275	0.95
	30	7	2.3	295	1.05
yes	20	8	1.7	320	0.8
	30		2.0	290	0.75
	40		2.3	270	0.7
	30	7	2.0	290	0.8

For $X > 25$, one can obtain a good fit with $R(\nu) = 1$. A Boltzmann plot in which the intensities of all observed lines are corrected for optical depth, beam filling, and different X, is shown in Fig. 12 and an examples of the dependence of the χ^2-sum on the model parameters is given in the panels of Fig. 13: with fixed Δv and X, we varied the source size (upper panel), column density (lower panel) and temperature and determined then the rest of the parameters to minimize the χ^2-sum applying also a correction for line broadening. The contours give the confidence levels of 1, 2 and 3σ for all six degrees of freedom which confine the source size to a range of 0.65″ to 0.85″ and the temperature

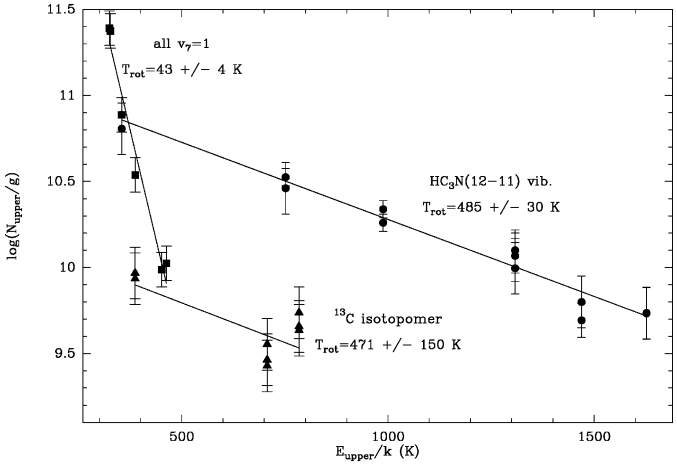

Fig. 11. Boltzmann plot of all detected lines of vibrationally excited HC_3N(12–11) in the observed band at 109 GHz (dots), all v_7 lines (squares) with different J, and all lines of ^{13}C isotopomer at 155 GHz (triangles). All intensities were corrected to match the 109 GHz beam by assuming a source size much smaller than the beams.

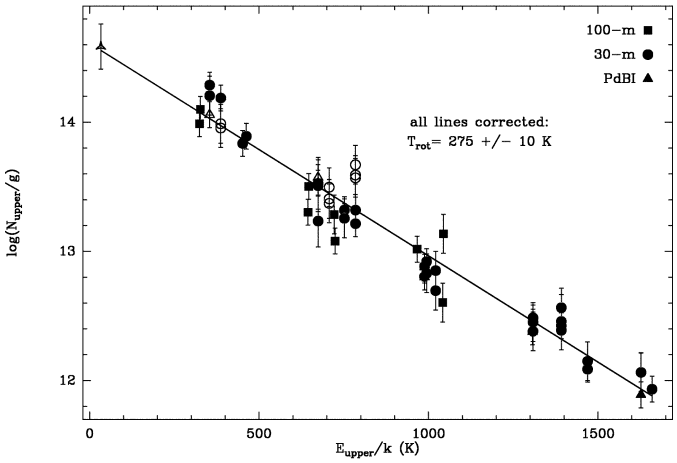

Fig. 12. Boltzmann plot of all vibrationally excited HC_3N lines corrected for optical depth (without taking line broadening into account) with a source size of 0.95″, an isotopomeric ratio of 40, and a line width of 8 km s^{-1}. Different Symbols are used for different telescopes. Filled markers denote lines from the main isotopomer, whereas empty markers denote lines from the ^{13}C and ^{15}N substituted isotopomer.

to a range of 240 K to 310 K for dust opacity solutions close to 0. The HC_3N column density is about 4×10^{18} cm^{-2}.

Smaller values of X lower the optical depths and accordingly the resulting column density, but increase the temperature. Without correcting for the line broadening due to optical depth effects, larger source sizes are needed to account for the intensity of the optical thick lines.

5.2. The excitation of the lines

All of these estimates rely on the assumption of LTE which is probably quite good in the light of the LTE fit which yielded to Fig. 12. But for a full understanding of the optical depth ef-

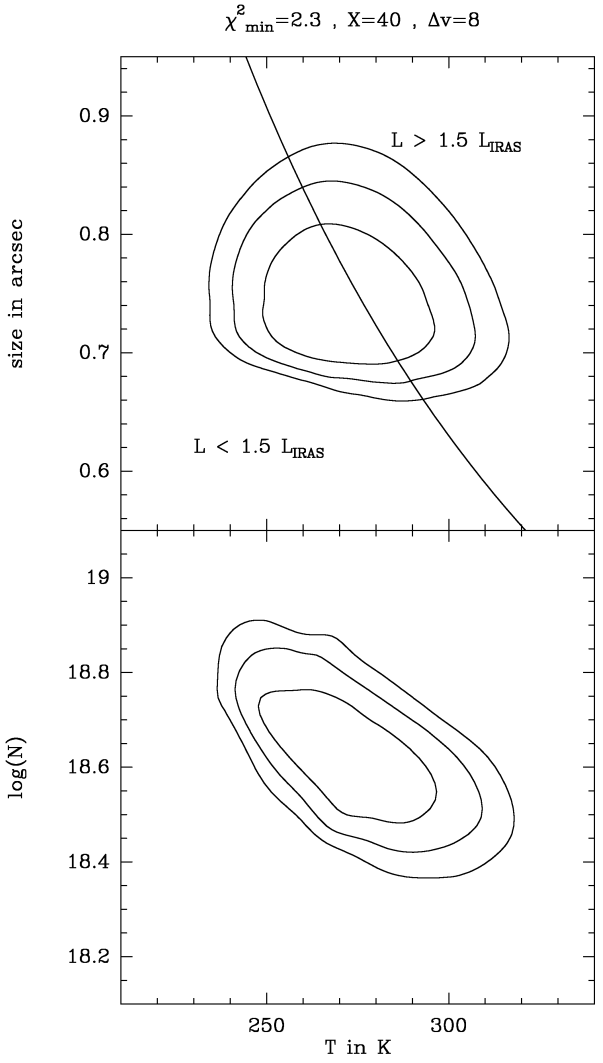

Fig. 13. Results of LTE analysis of the observed vibrationally excited HC_3N lines assuming a [^{12}C]/[^{13}C] ratio of 40, a linewidth of 8 km s^{-1} and using Eq. 8 to correct for optical depth line broadening. The contours give the confidence levels of 1, 2 and 3σ for six degrees of freedom. In the upper panel, the curve represents the loci of $L = 1.5\,L_{\rm IRAS}$ (see Sect. 6).

fects, a detailed modeling of the level population by statistical equilibrium calculation together with radiative transfer through a model cloud, is needed but would go beyond the objectives of the present analysis. Here, we just want to estimate whether the lines are populated mainly by collision or radiation. At the so-called critical density $n_{crit} = \beta A_{ul}/\gamma_{ul}$, where A_{ul} is the transition probability of spontaneous radiation, γ_{ul} the collisional rate coefficient and β the escape probability, collisional excitation can compensate for the radiative decay. Therefore, if the density is considerably lower than the critical density, only excitation by the radiation field can lead to population of the levels.

The radiative transition probability between vibrational states can be obtained by far-infrared absorption measurements. In the case of HC_3N this has been done by Uyemura & Maeda (1974) and Uyemura et al. (1982) for all the fundamental stretching and bending modes, respectively. The measured infrared intensities of the modes can then be converted to Einstein coefficients (see appendix of Deguchi et al. 1979) as has been done to produce Table 1.

Since no measurements or calculations of the collisional cross sections which change the vibrationally state of HC_3N are available, approximations have to be found. We have followed the suggestion of Goldsmith et al. (1982), who used the semi-empirical formula for vibrational relaxation times as a function of temperature, reduced mass, and energy of vibration in diatomic molecules given by Millikan & White (1963). With this relation, we calculated deexcitation cross sections. This is done for a temperature of 300 K and the resulting critical densities are shown in the last column of Table 1. The density in the hot core associated with G10.47+0.03 is of the order 10^7 cm^{-3} (Cesaroni et al. 1994; Wyrowski & Walmsley 1996) and therefore the vibrationally excited states cannot be populated collisionally, but require excitation by a strong IR radiation field unless strong radiative trapping in the infrared reduces the radiation probability to an effective value of $A_{ul}/\tau_{\rm IR}$ where the optical depth in the IR could exceed the radio optical depth by a factor 10 to 100 (Genzel 1992). This is likely for the HC_3N ν_7 state in extreme cases but not for more highly excited states.

6. Characteristics of the IR sources

Most of the critical densities of the IR transitions are much too high for them to be populated by collisions (cf. 5.2). Hence, they must be radiatively excited and therefore probe the IR radiation field of the observed sources at the pumping frequencies of the rotational lines. The total column densities involved ($10^{24} - 10^{25}$ cm^{-2}) lead to high optical depths in the infrared and the obtained vibrational temperatures of the IR levels are expected to measure the dust temperature.

One important property of an IR source is its total bolometric luminosity which can be derived from the IRAS fluxes. This luminosity gives us a constraint on the possible temperature and size of the source by applying the Stefan–Boltzmann law:

$$L_{\rm IRAS} \geq \pi\theta_S^2 d^2 \sigma T^4 \qquad (13)$$

θ_S is the source size, d the distance of the source, T the temperature and σ the Stefan–Boltzmann constant. With the IRAS luminosity $L_{\rm IRAS} = 5 \times 10^5$ L$_\odot$ for G10.47+0.03 (Cesaroni et al. 1994), this constrains the temperature for assumed source sizes of 2″ and 0.″5 to 140 and 390 K, respectively. It should be noted that this assumes spherical symmetry and that the luminosity for a disk-like geometry could be significantly smaller as discussed in Cesaroni et al. (1998).

Since the detection of ^{13}C species of HC_3N revealed that the v_7 lines of the main isotopomer are optically thick, we can use the brightness temperature of these lines to relate source size and temperature in another way:

$$T = T_{\rm L}\,\frac{\theta_B^2}{\theta_S^2} \qquad (14)$$

Here θ_B denotes the beam size. Combining both formulae, we can calculate for each observed v_7 line a unique source size and temperature (assuming equality in Eq. 13). The 3 and 2 mm lines lead to a size of 1.″25 and 175 K whereas the 1.3 mm lines result in a size of 0.″7 and 230 K.

Additionally, we used the luminosity constraint of Eq. 13 for our LTE fit. In Fig. 13 the range of forbidden source sizes and temperatures is marked with a curve, allowing for a 50% error in the IRAS luminosity. The source size is then constrained to values between 0.″65 and 0.″85.

However, we do not expect this combination of IR-source size and temperature to explain *all* observed vibrationally excited lines. For the excitation of the very high lying modes higher temperatures are necessary extending over smaller regions. The most likely scenario is an increase of temperature toward the interior of the source (see also Wyrowski & Walmsley 1996) in the high lying states of HC_3N. This can only be revealed by future sub arcsecond interferometer studies of these lines.

7. Conclusions

A sample of six hot core sources has been observed in vibrationally excited lines of HC_3N. Among the sources, G10.47+0.03 is unique in terms of high excitation molecular lines and revealed a panoply of new identifications of HC_3N in vibrationally excited states, even from ^{13}C isotopomeric forms of HC_3N. We derive an excitation temperatures of 250–330 K for the vibrationally excited HC_3N lines, depending on the assumed $^{12}C/^{13}C$ abundance ratio, though still higher temperatures may excite the highest lying modes of vibration. This vibrational temperature is consistent with the temperature found using $^{15}NH_3$ (Wyrowski & Walmsley 1996) and with the core temperature of the CH_3CN emission observed by Olmi et al. (1996b) but much higher than the peak brightness temperature of 120 K from the optically thick NH_3(4,4) line observed by Cesaroni et al. (1998). The latter inconsistency could be due to an unresolved clumped source structure which would reduce the observed brightness temperature of the ammonia observations.

The size of the IR source is found to be between 0.″65 and 1″. This is about half of the size determined from NH_3(4,4) and ground state CH_3CN emission but within the errors equal to the size of vibrationally excited CH_3CN emission (Cesaroni et al. 1998 and Olmi et al. 1996b). From the interferometer results we found the source of HC_3N emission to be coincident with NH_3(4,4) and CH_3CN within the positional error of 1″.

In this study many vibrationally excited states of HC_3N have been detected for the first time in interstellar space showing the valuable interrelation between laboratory spectroscopy and astrophysics and the particular usefulness of this molecule in tracing a wide range of rotational *and* vibrational excitation.

Acknowledgements. We would like to thank Carsten Kramer for help with the 30-m, Helmut Wiesemeyer for help with the PdBI observations and Frédéric Gueth and Karl Menten for a critical reading of the manuscript. FW has been partially supported by the Deutsche Forschungsgemeinschaft with grant number SFB 301. MW acknowledges travel support from CNR grant 97.00018.CT02 and ASI grant ARS-96-66. He also thanks the MPIfR for their hospitality during the time this article was in preparation.

Table 1. HNCO intensities in G10.47+0.03 observed with the 30-m

ν (MHz)	Trans.	Vib. state	$E_{\rm up}$ (K)	$\int T_{\rm MB}\,dv$ (K km s^{-1})
109871.952	$5_{24}-4_{23}$	v_0	188.9	8.5
109904.922	$5_{05}-4_{04}$	v_0	15.8	14.3
109495.200	$5_{15}-4_{14}$	v_0	59.0	7.7
110297.516	$5_{14}-4_{13}$	v_0	59.2	9.0
154414.181	$7_{16}-6_{15}$	v_0	72.9	20.1
110066.104	$5_{4}-4_{4}$	v_5	1539.8	0.3
110084.368	$5_{05}-4_{04}$	v_5	847.4	0.8
110089.690	$5_{3}-4_{3}$	v_5	1236.9	0.5
110104.112	$5_{24}-4_{23}$	v_5	1020.5	0.5
110105.356	$5_{23}-4_{22}$	v_5	1020.5	0.7
154090.197	$7_{4}-6_{4}$	v_5	1553.5	0.9
154114.411	$7_{07}-6_{06}$	v_5	861.1	3.7
154123.323	$7_{3}-6_{3}$	v_5	1250.6	2.9
154142.560	$7_{26}-6_{25}$	v_5	1034.2	3.3
154146.055	$7_{25}-6_{24}$	v_5	1034.2	3.8
110080.464	$5_{3}-4_{3}$	v_6	1355.4	0.4
110086.440	$5_{05}-4_{04}$	v_6	965.9	0.5
110164.245	$5_{14}-4_{13}$	v_6	1009.3	0.6
154110.119	$7_{3}-6_{3}$	v_6	1369.1	2.1
154119.019	$7_{07}-6_{06}$	v_6	979.6	2.1
154227.515	$7_{16}-6_{15}$	v_6	1023.0	4.0
109870.278	$5_{15}-4_{14}$	v_4	1178.0	blend
109961.242	$5_{05}-4_{04}$	v_4	1134.8	blend
154828.282	$7_{16}-6_{15}$	v_4	1191.9	0.7

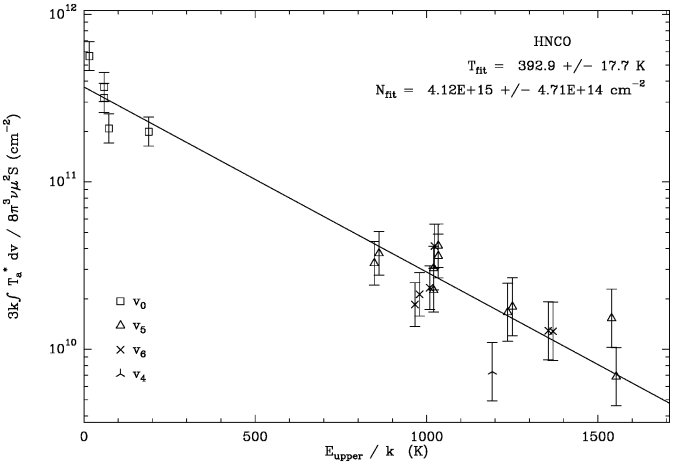

Fig. A1. Boltzmann plot of all detected lines of vibrationally excited HNCO. All intensities were corrected to match the 109 GHz beam by assuming a source size much smaller than the beams.

Appendix A: vibrationally excited HNCO

Toward G10.47+0.03, we report the first detection of vibrationally excited HNCO. Using the frequencies from labora-

tory measurements of Yamada (1977), a group of spectral line features in our 3 and 2 mm measurements can be attributed to HNCO in its v_4, v_5 and v_6 vibrational states which lie between 800 and 1100 K above ground (see Figs. 4 and 5). We checked line catalogs for possible blends with lines from other species but no blending lines were found. Integrated line intensities were derived from simultaneous Gaussian fits to all lines with the same J and are given in Table 1. To analyze the excitation of the lines, we used the line strengths of the ground state rotational transitions for the vibrational excited states as well. The resulting Boltzmann plot is shown in Fig. A1 and yields a temperature of 380 K, which should be regarded as an upper limit due to possible high optical depths of the lines with lower energies above ground and possible blends of high excitation lines with U-lines.

References

Blake G.A., Sutton E.C., Masson C.R., Phillips T.G., 1987, ApJ 315, 621

Blake G.A., Mundy L.G., Carlstrom J.E., et al., 1996, ApJ 472, L49

Cesaroni R., Churchwell E., Hofner P., Walmsley C.M., Kurtz S., 1994, A&A 288, 903

Cesaroni R., Hofner P., Walmsley C.M., Churchwell E., 1998, A&A 331, 709

Churchwell E., Wood D., Myers P.C., Myers R.V., 1986, ApJ 305, 405

Churchwell E., Walmsley C.M., Cesaroni R., 1990, A&AS 83, 119

Churchwell E., 1991, In: Lada C.J., Kylafis N. (eds.) The Physics of Star Formation and Early Stellar Evolution. NATO Asi

Clark F.O., Brown R.D., Godfrey P.D., Storey J.W.V., Johnson D., 1976, ApJ 210, L139

Dahmen G., Wilson T., Matteucci F., 1995, A&A 295, 194

Deguchi S., Nakada Y., Onaka T., 1979, Publ. Astron. Soc. Japan 31, 105

Garay G., Rodriguez L.F., 1990, ApJ 362, 191

Gaume R.A, Fey A.L, Claussen M.J, 1994, ApJ 432, 648

Genzel R., 1992, In: Burton W.B., Elmegreen B.G., Genzel R. (eds.) The Galactic Interstellar Medium, Springer, p. 275,

Goldsmith P.F, Krotkov R., Snell R.L., 1982, ApJ 260, 147

Goldsmith P.F, Krotkov R., Snell R.L., 1985, ApJ 299, 405

Guilloteau S., et al., 1992, A&A 262, 624

Hofner P., Churchwell E., 1996, A&AS 120, 283

Hofner P., Wyrowski F., et al., 1998 (in prep.)

Mallinson P.D., Fayt A., 1976, Molec. Phys. 32, 473

Mallinson P.D., de Zafra R.L, 1978, Molec. Phys. 36, 827

Mauersberger R., Henkel C., Wilson T.L., 1988, A&A 205, 235

Millikan R.C., White D.R., 1963, J. Chem. Phys. 39, 3209

Olmi L., Cesaroni R., Walmsley C.M., 1996a, A&A 307, 599

Olmi L., Cesaroni R., Neri R., Walmsley C.M., 1996b, A&A 315, 565

Snyder L.E., Buhl D., 1974, ApJ 189, L31

Stutzki J., Genzel R., Graf U.U., Harris A.I., 1989, ApJ 340, L37

Turner B.E., 1991, ApJS 76, 617

Turrel G.C., Jones W.D., Maki A., 1957, J. Chem. Phys. 26, 1544

Uyemura M., Maeda S., 1974, Bull. Chem. Soc. Japan 47, 2930

Uyemura M., Deguchi S., Nakada Y., Onaka T., 1982, Bull. Chem. Soc. Japan 55, 384

de Vicente P., 1994, Ph.D. Thesis, Universidad Complutense de Madrid

Wild 1995: The 30m Manual, IRAM Tech. Report 377/95

Wood D.O.S., Handa T., Fukui Y., et al., 1988, ApJ 326, 884

Wyrowski F., Walmsley C.M., 1996, A&A 314, 265

Wyrowski F., Hofner P., Schilke P., et al., 1997, A&A 320, L17

Wyrowski F., 1997, Ph.D. Thesis, University of Cologne

Yamada K.M.T., 1977, J. Mol. Spectr. 68, 423

Yamada K.M.T., Creswell R.A., 1986, J. Mol. Spectr. 116, 384

Ziurys L.M., Turner B.E., 1986, ApJ 300, L19